CHAPTER-2

THIN FILM DEPOSITION AND CHARACTERIZATION

Abstract

In this chapter, a brief description of the sputter deposition method and the importance of the process parameters in thin film deposition is first discussed. The details of the characterization techniques used such as, x-ray diffraction, field emission-scanning electron microscopy, atomic force microscopy, energy dispersive x-ray spectroscopy, UV-VIS-NIR spectrophotometer, four probe method and nanoindentation are presented in the second part.

2.1. Thin film deposition

2.1.1Thin film deposition techniques

The processes of thin film deposition are distinguished based on the nature of source material, the technique of vaporization and the processes of condensation. Processes that involve the use of a solid source material which is vaporized either by heating or energetic particle bombardment and finally condense as a films are called physical vapor deposition technique. If the source materials are gasses and condensation of films occurs as a solid by product of the chemical reaction, the process is called chemical vapor deposition. In solution based techniques, the precursor is directly applied to the substrate and then dried to realize a film of the desired material [102, 103].

2.1.2. Sputtering

Sputtering is a PVD thin film deposition technique that is extensively used for deposition of complex materials. The ejection of atoms from the surface of a material (the target) by bombardment with energetic particles is called *sputtering*. If ejection is due to positive ion bombardment, it is referred to as *cathodic sputtering*. The ejected or sputtered atoms can be condensed on a substrate to form a thin film. Sputtering is useful for many materials; especially compounds and alloys, since the composition of the film comes out nearly the same as that of the target [104]. It is also useful for materials, which cannot be evaporated easily.

2.1.3 Physics of sputtering:

Physical sputtering is driven by momentum exchange due to collision between ions in the gas phase and atoms in the material. The incident ions set off collision cascades in the target. As a consequence, cascades recoil and atoms reach the target surface with energy above the surface binding energy leading to ejection from the surface. Physical sputtering has a well-defined minimum energy threshold which is equal to or larger than the ion energy at which the maximum energy transfer of the ion to a sample atom equals the binding energy of a surface atom. This threshold typically is somewhere in the range 10–100 eV [105].

2.1.4 Mechanism of Sputtering:

A sputtering event is initiated by the first collision between incident ions and target surface atoms followed by the second and the third collisions between the target surface atoms. The displacement of target surface atoms will be more isotropic due to successive collisions and atoms may finally escape from the surface. Figure 2.1 shows the sputtering collision on the target surface.

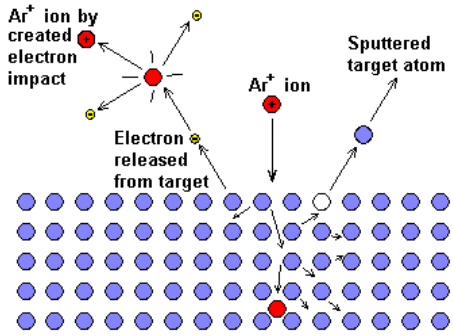

Figure 2.1 Incident ions and the sputtered particles [105]

Sputtering Yield:

The sputter yield *S* is defined as *the mean number of atoms removed from the surface of a material (target) per incident ion*. The sputtering yield is dependent on the following parameters [104]

i) Density of target material
ii) Energy of incident ion
iii) Incident angle of ions
iv) Crystal structure of target surface

Sputtering is classified into different types depending on the nature of target material (conducting, semiconducting or insulating); process used for ionization of the sputtering gas single or mixed gas sputtering atmosphere and the number of layers or elemental components in the thin films.

2.1.5 RF Magnetron Sputtering

Due to the substitution of an insulator target for the metal target in a dc diode sputtering system, the sputtering glow discharge cannot be sustained because of the immediate build-up of a surface charge of positive ions on the front of the insulator. To sustain the glow discharge with an insulator target, the dc voltage power supply is replaced by an RF power supply. This system is called an RF sputtering system. Presently the RF-sputtering system holds an important position in the field of deposition of thin films. A schematic view of an RF magnetron sputtering system is shown in figure. 2.2.

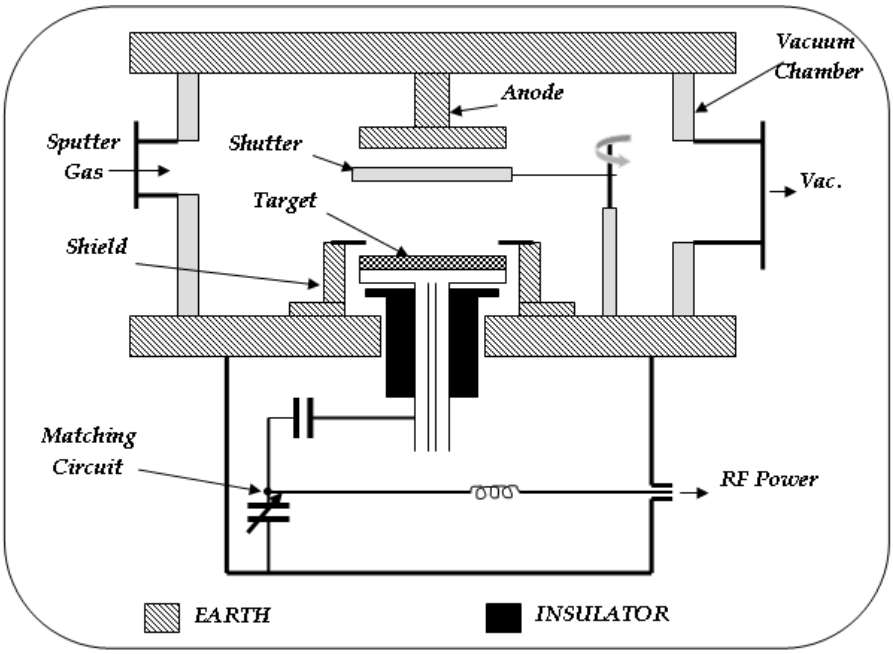

Figure 2.2 schematic view of an RF magnetron sputtering

The RF diode sputtering system requires an impedance-matching network between the power supply and discharge chamber. A typical network for impedance matching is shown in figure 2.3 [106].

The impedance of the RF-power supply is almost always 50 Ω. The impedance of the glow discharge is of the order of 1 to 10 kΩ. In RF diode sputtering, the target current density i_s is given by $i_s \cong C\frac{dV}{dt}$

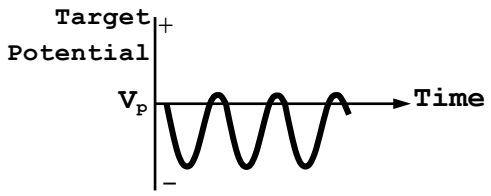

V_p: PLASMA POTENTIAL

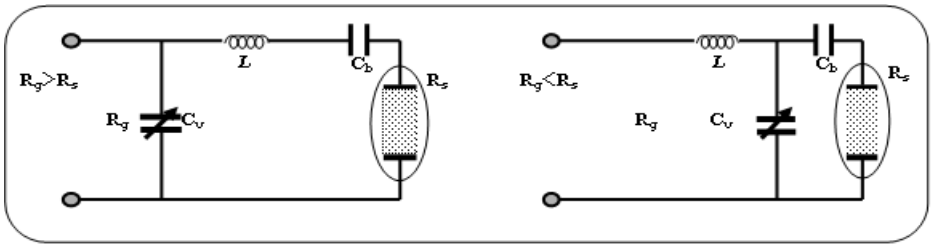

Figure 2.3 Impedance matching networks for RF-sputtering system

$$X_L = \sqrt{R_s R_g - R_s} \qquad X_c = \frac{R_s R_g}{X_L} \qquad X_c = R_s \sqrt{\frac{R_g}{(R_s - R_g)}} \qquad X_L = \frac{R_s R_g}{X_c}$$

R_g:impedance of RF-generator, C_v:variable capacitor

R_s:impedance of RF-discharge, C_v:blocking capacitor

where C is the capacitance between the discharge plasma and the target, $\frac{dV}{dt}$ denotes the time variations of the target surface potential. This indicates that the increase of frequency increases the target ion currents.

In the RF discharge system the operating pressure is lowered to as low as 1 mTorr, since the RF electrical field in the discharge chamber increases the collision probability between the secondary electrons and the gas molecules. In the RF sputtering system, a blocking capacitor is connected between the matching network and the target. The target area is much smaller than the grounded anode and the chamber wall. This asymmetric electrode configuration induces a negative dc bias on the target, and this causes sputtering in the RF system.

Magnetron sources are of great use to enhance ionization in the sputtering processes. In the magnetron, number of high strength magnets are placed at the rear of the target. They are fixed in a such a manner that the magnetic lines are force are perpendicular to the applied electric field.

As a result, the electron paths become helical, their mean free path increases and therefore ionization probability also increases. Figure 2.4 shows the cross-sectional view of the planar magnetron sputtering. Magnetron sputtering can be used in DC or RF modes to enhance sputtering rates. It is now a standard technique for deposition of thin films by sputtering.

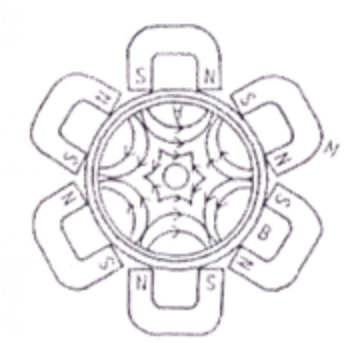

Figure 2.4 Cross-sectional view of the planar magnetron sputtering

In the magnetron sputtering system the working pressure is 10^{-5} to 10^{-3} Torr and the sputtered particles traverse the discharge space without collisions. Thus the deposition rate R is given by

$$R \cong k \frac{W_0}{t} \tag{1}$$

where $k=1$ for the planar system, W_0 is the amount of sputtered particles given by

$$W_0 = \left(\frac{j_+}{e} \right) st \left(\frac{A}{N} \right) \tag{2}$$

where j_+ is the ion current density at the cathode, e is the electron charge, s is sputter yield, A is atomic weight of sputtered materials, and N is Avogadro's number [104].

2.1.6 Reactive sputtering

To deposit metal thin films by sputtering, the sputtering process is carried out in an inert gas atmosphere (usually argon). However, to deposit compound thin films such as TiN, TiO_2, AlN it is required to introduce reactive gas, such as O_2, N_2 in the sputtering process. The gas will react with the growing film to form the desired compound and the process is called Reactive sputtering. A major disadvantage is that the reactions occur with the sputtering target surface as well. This 'target poisoning' complicates reactive sputtering and reduces the thin film growth rate [107-109]. A few other key points in reactive sputtering process are

1) Part of the reactive gas is exhausted through the pumps while the rest react with the growing film.
2) Compounds tend to sputter more slowly than metals.
3) Target hysteresis-as shown in figure 2.5. This is characterized by sudden jumps in the thin film deposition rate, target voltage or nitrogen pressure. To successfully make compound thin films by reactive sputtering we must stay away from these sudden jumps in the process.

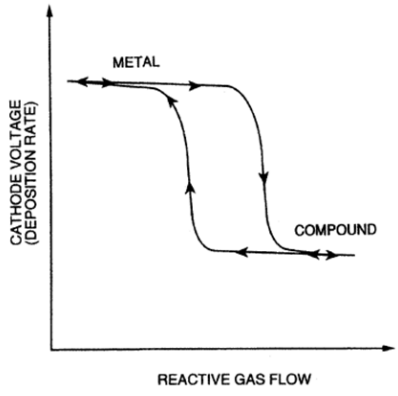

Figure 2.5 Hysteresis in reactive sputtering

2.1.7 Deposition of Ti, TiN_x and $Ti_{1-x}Nb_xN$ films using RF reactive magnetron sputtering

RF magnetron sputtering has been widely accepted as one of the versatile techniques for the deposition of high quality TiN thin films by several research groups [110-113]. Using RF magnetron sputtering any solid material (metal, insulator and semiconductor) can be sputtered. In addition, complex compounds can be sputtered stoichiometrically, use of low gas pressure for sputtering, appreciable rates of deposition and uniformity over large area is also possible. The properties of the sputter films are strongly influenced by process parameters such as RF power density, substrate temperature, working/sputtering gas pressure and substrate to target distance. In the present study, metallic Ti thin films were deposited in 100% Ar atmosphere, while TiN and $Ti_{1-x}Nb_xN$ films were deposited in 100% N_2 atmosphere.

During deposition of thin films, the vacuum chamber is continuously cooled by flow of water through the water cooling jackets fitted on the exterior to the vacuum chamber. It is evacuated through the electro-pneumatic roughing valve from atmospheric pressure to 2×10^{-2} mbar using a rotary vane mechanical pump (RP, DS-102, Varian, Italy) with an approximate pumping speed of $6.84 m^3h^{-1}$. The vacuum chamber is isolated from the turbo molecular pump (TMP, Turbo-V 301, Varian, Italy) through a mechanical screw driven gate valve which is attached to the vacuum chamber by a 6" conflat flange. The pumping speed of the TMP is about 15 m^3h^{-1}. Once the chamber pressure reaches to 2×10^{-2} mbar, the roughing valve is closed and the TMP is evacuated through electro-pneumatic backing valve. As the fore-line pressure reaches to 2×10^{-2} mbar, the TMP is switched on and the gate valve is opened. The

pressure in the vacuum chamber can now be brought into the high vacuum regime. The pressure is monitored using a cold cathode gauge. A base pressure of 3×10^{-6} mbar can be achieved in about 2 hours. The working pressure during is controlled partly by adjusting the total input gas flow and by reducing the throughput of the TMP by partially closing the gate valve. Once the pre-determined working pressure and deposition temperature is achieved, the sputter deposition process is started by initiating the plasma using the RF power generator coupled with matching network. The vacuum chamber walls and substrate holding stage was grounded during deposition. The experimental conditions used to deposit Ti, TiN_x and $Ti_{1-x}Nb_xN$ are mentioned in chapters 3, 4 and 5. Figure 2.6 shows the photograph of the RF magnetron sputtering system (Advanced Process Technology, Pune, India) used in the present study.

Figure 2.6 Photograph of the RF reactive magnetron sputtering used in the present study

2.1.8 Substrate material and preparation

In this study, the films were deposited on to different substrates depended on the nature of study. Optical (transmittance and reflectance) and photoluminescence studies TiN_x were carried out on films deposited on to well polished fused silica substrates which were 25 mm^2 in area and 0.5 mm thick. For hardness measurements, $Ti_{1-x}Nb_xN$ films were deposited on mirror polished 316 LN nuclear grade stainless steel substrates of 25 mm^2 area and 2 mm thick. Prior to deposition the substrates were cleaned with a laboratory detergent, wiped with soft dust free surgical cotton, and then washed with tap water. Traces of detergent were removed by gently rubbing under running water, then the substrates were rinsed in distilled water. These substrates were dried in an oven at 100^oC. Finally the substrate was cleaned by rinsing in an ultrasonic bath of acetone, iso-propanol and de-ionized water for about 15 minutes each. Again the cleaned substrates were finally dried in an oven at 100^oC for 30 min.

2.2. Characterization

2.2.1. Thickness measurement: Surface profilometer

The thickness of the samples was measured using stylus profiler (also known as profilometer) (Model XP-1, Ambios Technology, USA). Surface profilometry is a direct, simple and fast measurement technique for determining the physical thickness of thin films [114]. The only requirement is the existence of a step as shown in figure 2.7. Diamond stylus (tip) was used to determine the thickness of Ti, TiN_x and $Ti_{1-x}Nb_xN$ films.

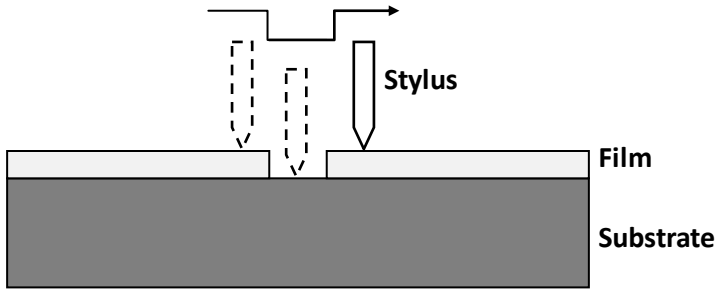

Figure 2.7 Illustration of stylus profilometer measure film thickness

2.2.2. Structural characterization

X-ray diffraction is a well-known technique for characterizing the crystal structure of materials. X-rays have a wavelength of the order of Angstroms (10^{-10} m), which is comparable to the inter-atomic spacing in crystalline solids. Therefore, a diffraction pattern can be observed when a beam of x-rays is directed on a crystalline material (where the atoms are arranged periodically). This diffraction pattern is directly related to the crystal structure of the material under observation.

The crystal structure of Ti, TiN_x and $Ti_{1-x}Nb_xN$ films was determined using x-ray diffraction and transmission electron microscopy. Two types of x-ray diffractometers with different x-ray source were used to characterize the films. One was equipped with Co K_α (λ=1.7889A^o) radiation in a wide angled x-ray diffractometer (INEL, CPS120) and a curved position sensitive detector was used to collected the data. The diffractometer is in Bragg-Brentano geometry. While, the other is grazing-incident x-ray diffrctometer (Bruker D8 Discovers) equipped with Cu K_α radiation (λ=1.5405A^o). The GI-XRD pattern was obtained

with a grazing angle of 1.5°. Calibration using a Si standard was done to account for the instrumental line broadening and the values were approximately 0.05° for INEL and 0.10° for Bruker diffractometer. The XRD and GIXRD patterns of all films were indexed using joint committee on powder diffraction standards (JCPDS) [115. 116]. These results gave important information regarding the variation in film orientation, lattice constant, crystallite size and strain as a function of process parameters.

Crystallite size and lattice parameter calculation

The crystallite sizes of the films were calculated by a line profile analysis of the peak broadening. The crystallite size *D* was estimated using the Scherrer equation [117].

$$D = \frac{0.94\lambda}{\beta \cos\theta_{\beta}} \tag{3}$$

Here λ is the x-ray wavelength (Cu-K_{α} radiation, λ=0.15405 nm), β is full width at half-maximum of the XRD peak and θ is the Bragg diffraction angle.

The lattice parameter was calculated using 2θ peak position from the relation

$$d_{hkl} = \frac{a}{\sqrt{h^2 + k^2 + l^2}} \tag{4}$$

Where
a - lattice constant
d- spacing between the planes
h,k,l- miller indices

Vegard's law

Vegard's is an approximate empirical rule which has a linear relation between the lattice parameter and the composition of the ternary system. In the case of $Ti_{1-x}Nb_xN$ thin films, the calculated lattice parameter of cubic structure was compared with the expected value from Vegards law [118]

For the ternary system, $Ti_{1-x}Nb_xN$, it is expressed as

$$a_{Ti_{1-x}Nb_xN} = (1-x)a_{TiN} + xa_{NbN} \quad (5)$$

Here a_{NbN} and a_{TiN} are the bulk values of the lattice parameters of NbN (0.439 nm) and TiN (0.424 nm) respectively.

2.2.2.2. Transmission Electron Microscopy (TEM)

The crystal structure of TiN_x and $Ti_{1-x}Nb_xN$ thin films were also determined using transmission electron microscope operated in the selected area electron diffraction (SAED) mode (model: FEI Tecnai G^2 S-Twin, FEI electron microscope operated at 200 kV using Gatan CCD camera).

Figure 2.8. Photograph of the Transmission electron microscope

2.2.3. Chemical composition

Chemical composition of TiN_x and $Ti_{1-x}Nb_xN$ thin films was determined using x-ray photoelectron spectroscopy and energy-dispersive x-ray spectroscopy respectively.

2.2.3.1 X-ray photoelectron spectroscopy

X-ray photoelectron spectroscopy (XPS) is a quantitative spectroscopic technique that measures the elemental composition, chemical state and electronic state of the elements that exist within a material. The phenomenon is based on the photoelectric effect, where the concept of the photon was used to describe the ejection of electrons from a surface when photons impinge upon it. XPS

simultaneously measure the kinetic energy and number of electrons that escape from the top 1 to 10 nm of the material being analyzed. Each atom in the surface has core electrons with a characteristic binding energy that is conceptually, not strictly, equal to ionization energy of the electron. The energy of an X-ray with particular wavelength is known, the electron binding energy of each of the emitted electrons can be determined by using an equation

$$E_{binding} = E_{photon} - (E_{kinetic} + \phi) \quad (6)$$

where E_{binding} is the binding energy (BE) of the electron, E_{photon} is the energy of the X-ray photons being used, E_{kinetic} is the kinetic energy of the electron as measured by the instrument and φ is the work function of the spectrometer [119]. The binding energy of the peaks is characteristic of each element. The peak areas can be used (with appropriate sensitivity factors) to determine the composition of the materials surface. The shape of each peak and the binding energy can be slightly altered by the chemical state of the emitting atom.

In the present case, the composition of TiN_x films, *i.e.*, the N/Ti ratio in the films was determined using X-ray photoelectron spectrometer (XPS-model PHI 5700). The excitation X-ray source for the XPS used was Mg K_α at an energy level of 1253.6 eV. The spectra of the Ti-2p, N-1s, and O-1s peaks were calibrated with respect to the C-1s peak, which resulted from the adventitious hydrocarbon at an energy level of 284.8 eV. The base pressure in the analysis chamber was about 7×10^{-8} Pa. The XPS spectra were fitted using a non-linear least squares fit assuming a Gaussian/Lorentzian peak shape (G/L mixing ratio = 0.3).

2.2.3.2 Energy dispersive x-ray spectroscopy

Energy Dispersive X-Ray Spectroscopy (EDS or EDX) is a chemical microanalysis technique used in conjunction with scanning electron microscopy (SEM). The EDS technique detects x-rays emitted from the sample during bombardment by an electron beam to characterize the elemental composition of the analyzed volume. Features or phases as small as 1 μm or less can be analyzed. When the sample is bombarded by the SEM's electron beam, electrons are ejected from the atoms comprising the sample's surface. The resulting electron vacancies are filled by electrons from a higher state, and an x-ray is emitted to balance the energy difference between the two electrons' states. The x-ray energy is characteristic of the element from which it was emitted [120].

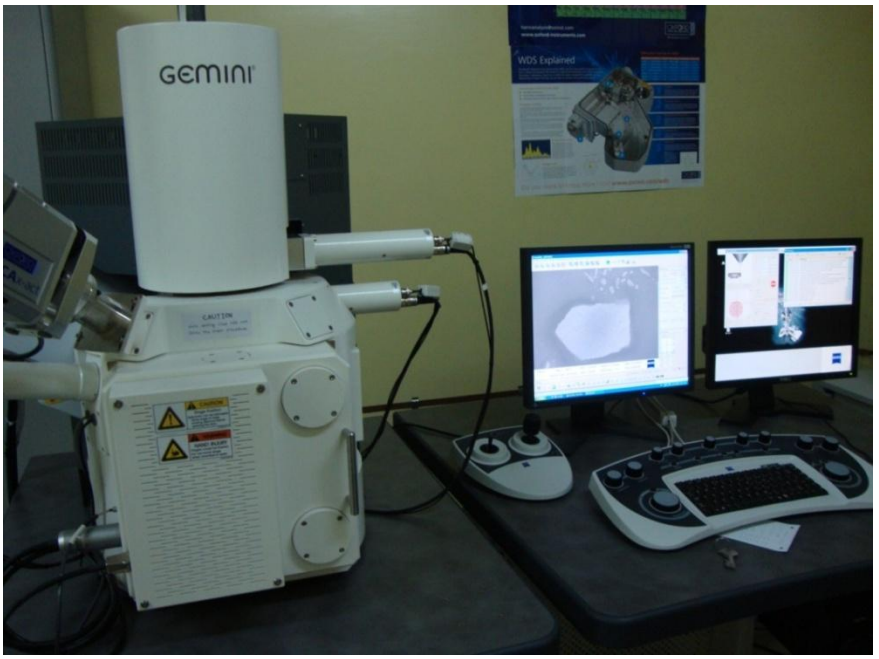

Figure 2.9 Photograph of field-emission scanning electron microscopy attached with INCA EDX detector. The present system used to determine microstructure and composition of the films.

In the present study, chemical composition of $Ti_{1-x}Nb_xN$ films was determined using energy-dispersive x-ray spectroscopy (EDX) analysis. EDX spectrum is obtained from FE-SEM using an INCA EDX system, which is equipped with an Oxford Instruments. The operating voltage and working distance for EDX measurement is 20 kV and 8.5 mm respectively.

2.2.4. Optical characterization

Optical properties of Ti, TiN_x and $Ti_{1-x}Nb_xN$ thin films were studied using a JASCO (V-570 UV-VIS-NIR) double beam spectrophotometer. The optical properties of these films are studied with respect to their transmittance and reflectance spectra by considering the interaction of photon with matter and consequent changes in electronic states The spectral transmission and reflectance (near normal) in the wavelength region from 190 to 1500 nm. The optical constants, refractive index and extinction coefficient of TiN_x thin films was calculated by fitting the measured reflectance/transmittance spectra using PUMA (Pointwise Unconstrained Minimization Approach) software [121, 122]. While refractive index and extinction coefficient and dielectric function of $Ti_{1-x}Nb_xN$ thin films was calculated by fitting the measured reflectance spectra based on Drude-Loerntz model [123].

If light is incident on a film of refractive index, n, coated onto a substrate of refractive index s, then at the air-film, the film-substrate and substrate-air interfaces, part of the incident intensity is reflected and part is it is transmitted. From fundamental considerations of optics it follows that since the reflected and transmitted beams originates from a single coherent source, the beams will exhibits interference

effects. The schematic diagram of the optics is shown in figure 2.10. The reflectance and transmittance spectra collected from the spectrophotometer were analyzed and studied the optical properties.

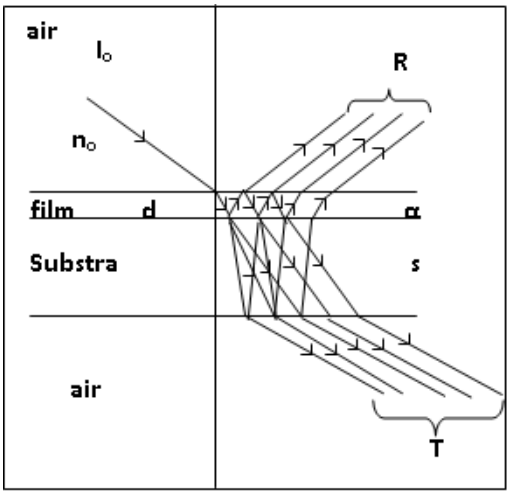

Figure.2.10 Interference from a thin film on a thick substrate, s>>d

If I_0 is the incident light and I the intensity of light after passing through the sample then, from *Beer's law* [124]

$$I = I_0 e^{-\alpha t} \tag{7}$$

Where, α is the absorption coefficient of the sample and t is the thickness of the sample.

The spectra transmittance and reflectance (at 6^0 angle of incidence) of the films were measured using a UV-VIS-NIR double beam spectrophotometer with an accuracy of ±0.2%. Before recording the spectra, a 100% base line was established by performing the back correction. The wavelength range of the instrument was 190 to 2500 nm.

The spectra reflectance curves were taken using a Aluminum mirror (provided by the supplier) as the reference.

The transmittance of the samples is given by

$$T = \frac{I}{I_0} \tag{8}$$

Reflectance is given by

$$R = (n-1)^2 + \frac{k^2}{(n+1)^2} + k^2 \tag{9}$$

and the absorption coefficient α is defined by

$$\alpha = \frac{4\pi k}{\lambda} \tag{10}$$

So, equation 9 becomes, with the substitution of k from equation (4),

$$n = \frac{(1+R)}{(1-R)} \pm \left\{ \left(\frac{R+1}{R-1} \right)^2 - (1+k)^2 \right\}^{\frac{1}{2}} \tag{11}$$

Furthermore, optical constants n and k of thin films are highly influenced by various factors like deposition rate, substrate temperature, film thickness, microstructure, crystallinity and chemical composition

2.2.5 Microstructural characterization

The microstructure of Ti, TiN_x and $Ti_{1-x}Nb_xN$ thin films were determined using field emission-scanning electron microscopy (Carl ZEISS, FEG, Ultra 55) and atomic force microscopy (Seiko Instruments, SPA-400 of 3800 probe station, Japan) respectively. The FE-SEM images were obtained at an operating voltage of 20 kV and the working distance is 8.5 mm. The AFM images were registered in a contact mode with Si

cantilevers of length 100µm. The resonant frequency and spring constants of the cantilever is 13 kHz and 0.18 N/m respectively.

2.2.5.1 Field Emission-Scanning Electron Microscopy (FE-SEM)

The scanning electron microscopy is a versatile technique that reveals detailed information about the morphology and the composition of natural and manufactured materials. SEM rasters a focused electron beam across a sample surface, providing high-resolution and long-depth-of-field images of the sample surface. A field-emission SEM provides narrower probing beams at low as well as high electron energy, resulting in both improved spatial resolution and minimized sample charging and damage [125]. The emission is reached by placing the filament in a huge electrical potential gradient. The FEG is usually a wire of Tungsten (W) fashioned into a sharp point. The significance of the small tip radius (~ 100 nm) is that an electric field can be concentrated to an extreme level, becoming so big that the work function of the material is lowered and electrons can leave the cathode. FESEM uses Field Emission Gun producing a cleaner image, less electrostatic distortions and spatial resolution < 2nm (that means 3 or 6 times better than SEM). The images formed by the field emission scanning electron microscope are from secondary electrons, backscattered electrons, characteristic X-rays, Auger electrons and others that are emitted by the sample.

2.2.5.2 Atomic force microscopy

Atomic force microscopy (AFM) is a very high-resolution type of scanning probe microscopy. SPM images are obtained by scanning a sharp probe across a surface while monitoring and compiling the tip-sample interactions to provide an image. The measurement of local physical properties of the material is extremely important for semiconductor fabrication. Using the SPM technique one can study the local physical properties materials down the atomic scale. The resolution obtained by this technique can resolve the single atom and the map the real 3-D images of the surface [126, 127].

2.2.5.3 Conductive-Atomic force microscopy

Conductive-Atomic Force Microscopy (C-AFM) is a mode of atomic force microscopy in which a conductive tip is scanned in contact with the conductive sample surface, while a voltage is applied between the tip and the sample, generating a current image. Using (C-AFM) one can probe the local variations in the conductivity of a material (crystal or thin film) with microstructure and thus examine the local variation of current at grain and grain boundaries [128-131].

The C-AFM measurements were made on the surface of TiN and $Ti_{1-x}Nb_xN$ thin films in order to study the local electron transport and microstructure origin of the conductivity. The C-AFM measurements were standardized first using a platinum thin film deposited on a silicon substrate. The C-AFM was operated in the constant force contact mode with Si cantilevers. The tip and one side of the cantilever were coated with 25 nm Au layer. The length of the cantilever is 10 μm, with a spring

constant of 2.2 N/m and resonant frequency of 29 kHz. The radius of curvature of the tip is less than 35 nm. The sample stage and the cantilever are carefully insulated from the apparatus frame. Conductive silver paint pasted on the top surface of the films formed the other electrode, to which a bias voltage was applied. The conductive tip was the counter microelectrode, connected to the ground potential. The feedback signal is used to generate a normal contact AFM topography image, while the current passing between the sample and the tip generates the conductive AFM (current) image. When surface morphology and local current are registered simultaneously, a dc voltage of 1V is applied to the bottom electrode prior to scanning. The range of current, which the current preamplifier could measure, was 100 pA to 100 nA. For each film a new tip was used to avoid artifacts due to tip erosion. A schematic view of the C-AFM measuring set-up is shown in figure 2.11.

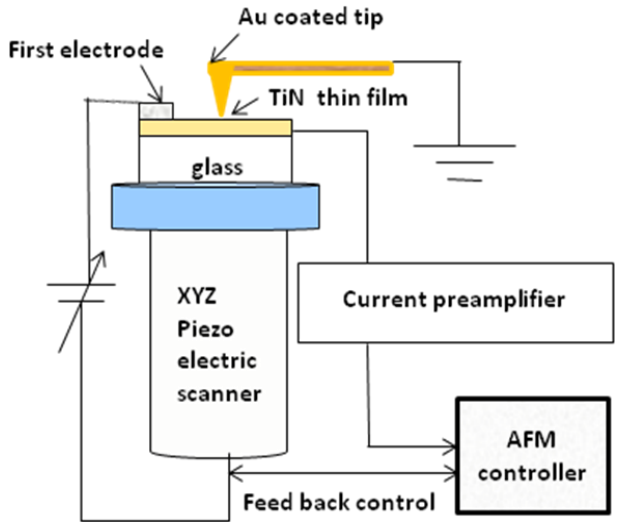

Figure 2.11 Schematic diagram of the conductive atomic force microscopy measuring set-up

In the present case, we have used SPA 400 of SPI 3800 probe station of Seiko Instruments, Japan for both contact mode and current mode.

Figure 2.12 Photograph of the SPA-400 atomic force microscopy used in the present study

2.2.6 Four probe method: measurement of electrical resistivity

Surface resistivity could be defined as the material inherent surface resistance to current flow multiplied by the ratio of specimen surface dimensions (width of electrodes divided by the distance between electrodes) which transforms the measured resistance to that obtained if the electrodes had formed the opposite sides of a square. In other words, it is a measure of the material surface inherent resistance to current flow.

Surface resistance does not depend on the physical dimensions of the material [132]. Four probe technique is very useful to measure the electrical resistivity of thin metallic and semiconductors films. The schematic diagram of four probe method used to measure the resistivity of Ti, TiN_x and $Ti_{1-x}Nb_xN$ films is shown in figure 2.13. The four probe measurement were carried out in a Agilent Technology B1500A, semiconductor analyzer,

According to Ohm's law, the resistance (R) of a material is the applied voltage (V) divided by the current (I) drawn across the material across two electrodes.

R=V/I

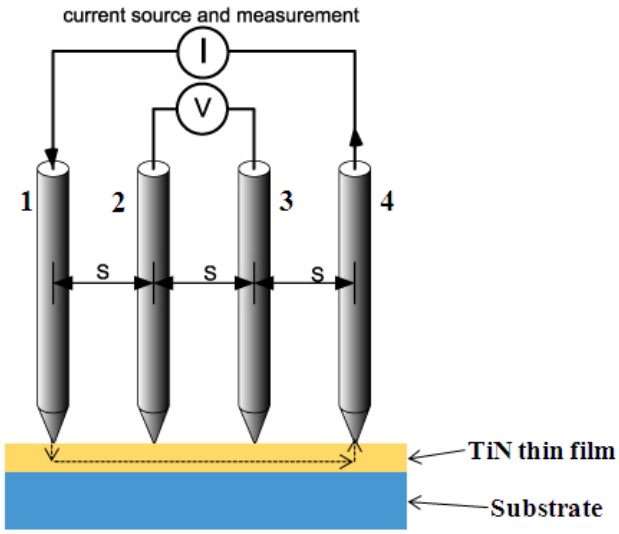

Figure 2.13 The schematic diagram of four probes set up. Probes 1 and 4 carry current (I), probes 2 and 3 measure voltage (V).

In the four-point probe set up, the voltage potential V adjacent to a probe carrying current can be given by

$V=\rho I/2\pi r$

Where ρ is the surface resistivity of a material of semi-infinite size, I is the current in the probe and r is the distance between the voltage and the current probes.

Using dimensions in Figure 2.13 the voltage at probe 2 is,

$V_2= \rho I/2\pi \{(1/S_1)-(1/(S_2+S_3))\}$

The voltage at probe 3 is

$V_3= \rho I/2\pi \{(1/(S_1+S_2)) - (1/S_3)\}$

To get total voltage, substrate the voltage V_2-V_3

$V = = \rho I/2\pi \{(1/S_1)+ (1/S_3)- (1/(S_2+S_3))- (1/(S_1+S_2))\}$

Rearranging to get the resistivity

$\rho = 2\pi V/I /\{(1/S_1)+ (1/S_3)- (1/(S_2+S_3))- (1/(S_1+S_2))\}$

However, if all probe spaces are an equal size s, then the equation become

$\rho = 2\pi s (V/I)$

Considerations that need to be account for accurate four-point probe measurements are the spacing of the probes, temperature effects, thickness and surface roughness of the film. Therefore, the resistivity of metallic and semiconductor thin films measured using four probe method is

$\rho = 2\pi s (V/I) \times C.F$

In the above equation the correction factor (C.F) arises due to film thickness and surface roughness.

2.2.7. Mechanical characterization

Mechanical properties of film such as hardness (H), Young's modulus (Y), yield stress (σ) and ultimate tensile stress (σ_{UTS}) are derived from the response to applied force. In the present study, nanomechanical properties such as hardness and Young's modulus and nanotribological properties such as friction coefficient and wear volume were determined using nanoindentation, nanoscratch and wear test respectively. All above tests were performed in a Hysitron nanomechanical system (TriboIndentor, 900 series, USA).

2.2.7.1 Nanoindentation

Nanoindentation is a simple method that consists of hard indenter, indenting a specimen by a very small load using a high precision instrument, which records the load and displacement continuously [133]. The mechanical properties of thin films up on nanoindentation can be derived from the measured load-displacement (or loading /unloading) curve through appropriate analysis.

Hardness H of a material is usually defined as its resistance to local plastic deformation when a force is applied. As load is applied to the indenter, the depth of penetration in to the sample is measured. An indentation test instrument provides experimental results in the form of a load-displacement curve for the loading and unloading part of the indentation process as shown in figure 2.14

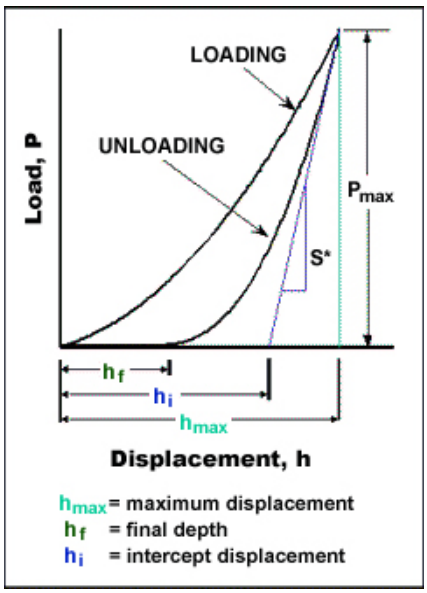

igure 2.14 Example of nanoindentation load-displacement curve obtained from Berkovich indenter during loading and unloading (32).

An analysis of the unloading data provides a value for the depth of the area of contact at full load. The area of contact at full load is determined from the known angle or radius of the indenter. For Berkvoch tip the total included angle on this tip is 142.3°, with a half angle of 65.35°. The hardness is derived by dividing the maximum load (P_{max}) by area of contact (A), thus [133]

$$H = \frac{P_{max}}{A(h_c)} \tag{12}$$

The slope of the linear variation of the unloading curve measures the elastic stiffness (S).

$$S = \frac{dp}{dh} = \frac{2}{\sqrt{\pi}} E_r \sqrt{A(h_c)} \tag{13}$$

Here E_r is the reduced modulus of the material. The Youngs modulus (Es) can be calculated using the equation

$$\frac{1}{E_r} = \frac{(1-\nu_i^2)}{E_i} + \frac{(1-\nu_s^2)}{E_s} \qquad (14)$$

In the above equation υ and E stands for poisson's ration and Young modulus of indenter and sample. The subscript i and s represents the *indenter* and *sample* respectively.

In the present case, Ti, TiN_x and $Ti_{1-x}Nb_xN$ films were indented by Berkovich-type pyramidal diamond tip with a maximum load of 2000 μN. The trapezoid load function (which includes the loading, holding and unloading segments) was used to measure the hardness of the films with a loading rate of 200 μNs^{-1} and segment time of 10 see for each segment.

2.2.7.2 Scratch test

Scratch test method is intended to measure the resistance of solid surfaces to permanent deformation due to friction from a sharp stylus tip. In thin film-substrate system, using scratch test one can quantify parameters such as friction coefficient and adhesive strength [134, 135]. This technique involves that generate a controlled scratch by dragging a tip across the film surface under a constant or incremental normal load. In a scratch test, both lateral and normal loads applied simultaneously to the indenter in order to get scratch length of few micrometers. The basic principle involved in scratch is represented in figure 2.15. At a certain critical load the film surface will start to deform. The critical loads are very precisely detected by means of an acoustic sensor. The critical load data is used to quantify the adhesive properties of different film - substrate combinations.

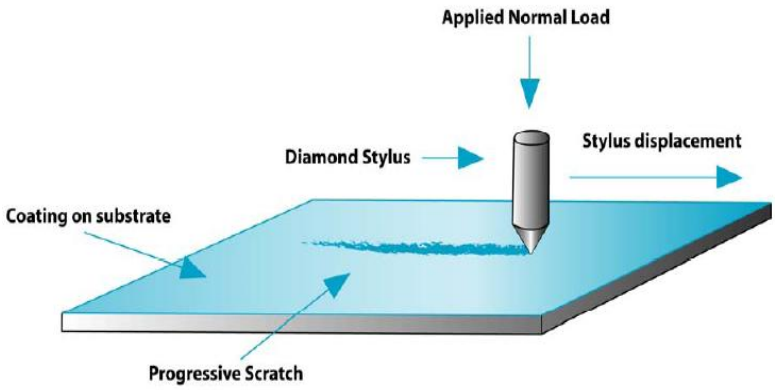

Figure 2.15 Principle of scratch test

The coefficient of friction is defined as the ratio of lateral force to normal force applied to the indenter (F= μL). In a scratch test, the coefficient of friction can simply determined by dividing the lateral force to that of normal force.

2.2.7.3 Wear test

The definition of wear may include loss of dimension from plastic deformation if it's originated at the interface between two sliding surfaces. The material intrinsic surface properties such as hardness, strength, ductility, work hardening etc. are very important factors for wear resistance [134-136]. To do wear test a specific area should be defined on the surface of the sample and the data was analyzed in terms of wear depth and wear volume. Wear volume can be calculated from the relation.

$$\text{Wear volume} = (\text{wear area})^2 \times (\text{wear depth}).$$

The variation in wear volume could be used to define the wear behavior of the material.

In the present case, a conical tip was used for both scratch and wear test of $Ti_{1-x}Nb_xN$ thin films. In the scratch test 5 segments were used in the load function to apply both lateral and normal loads with a scratch ramp force from 0 to 5000μN. Normal force and lateral displacements are controlled, while lateral force and normal displacement are simultaneously recorded as a function of time. During wear test, tip is repeatedly scanning over 2 μm × 2 μm area with a contact force of 80 μN). In addition to mechanical and tribological tests, Hysitron nanomechanical system also has the imaging capability using *in-situ* atomic force microscopy. *In-situ* atomic force microscopy is employed to visualize the scratch and wear behavior

Figure 2.16 photograph of the Hysitron (Triboindentor-900) nanomechanical test system